The Ocean Colour Climate Change Initiative: II. Spatial and temporal homogeneity of satellite data retrieval due to systematic effects in atmospheric correction processors

Dagmar Müller [a,*], Hajo Krasemann [a], Robert J.W. Brewin [b], Carsten Brockmann [c], Pierre-Yves Deschamps [d], Roland Doerffer [a], Norman Fomferra [c], Bryan A. Franz [e], Mike G. Grant [b], Steve B. Groom [b], Frédéric Mélin [f], Trevor Platt [b], Peter Regner [g], Shubha Sathyendranath [b], François Steinmetz [d], John Swinton [h]

[a] Helmholtz-Zentrum Geesthacht, Max-Planck-Straße 1, 21502 Geesthacht, Germany
[b] Plymouth Marine Laboratory (PML), Prospect Place, The Hoe, Plymouth PL1 3DH, UK
[c] Brockmann Consult, Max-Planck-Straße 2, D-21502 Geesthacht, Germany
[d] HYGEOS, 165 Avenue de Bretagne, 59000 Lille, France
[e] NASA Goddard Space Flight Center, Greenbelt, MD, USA
[f] European Commission, Joint Research Centre, Institute for Environment and Sustainability, Ispra 21027, Italy
[g] European Space Agency, ESRIN, Via Galileo Galilei, Casella Postale 64, 00044 Frascati, Italy
[h] Telespazio VEGA UK Ltd., 350 Capability Green, Luton, Bedfordshire LU1 3LU, UK

ARTICLE INFO

ABSTRACT

The established procedure to access the quality of atmospheric correction processors and their underlying algorithms is the comparison of satellite data products with related in-situ measurements. Although this approach addresses the accuracy of derived geophysical properties in a straight forward fashion, it is also limited in its ability to catch systematic sensor and processor dependent behaviour of satellite products along the scan-line, which might impair the usefulness of the data in spatial analyses.

The Ocean Colour Climate Change Initiative (OC-CCI) aims to create an ocean colour dataset on a global scale to meet the demands of the ecosystem modelling community. The need for products with increasing spatial and temporal resolution that also show as little systematic and random errors as possible, increases. Due to cloud cover, even temporal means can be influenced by along-scanline artefacts if the observations are not balanced and effects cannot be cancelled out mutually.

These effects can arise from a multitude of results which are not easily separated, if at all. Among the sources of artefacts, there are some sensor-specific calibration issues which should lead to similar responses in all processors, as well as processor-specific features which correspond with the individual choices in the algorithms.

A set of methods is proposed and applied to MERIS data over two regions of interest in the North Atlantic and the South Pacific Gyre. The normalised water leaving reflectance products of four atmospheric correction processors, which have also been evaluated in match-up analysis, is analysed in order to find and interpret systematic effects across track. These results are summed up with a semi-objective ranking and are used as a complement to the match-up analysis in the decision for the best Atmospheric Correction (AC) processor.

Although the need for discussion remains concerning the absolutes by which to judge an AC processor, this example demonstrates clearly, that relying on the match-up analysis alone can lead to misjudgement.

© 2015 Elsevier Inc. All rights reserved.

1. Introduction

Among the essential climate variables (ECV) – which have been defined within the Global Climate Observation System (GCOS-154 (2011), GCOS) – ocean colour products in terms of water leaving radiance (or reflectance) can be found. The GCOS requirements suggest the goal of 1 km horizontal resolution with daily observations in order to address scientific questions in a climate change background including mesoscale processes. It is a goal of the OC-CCI project to provide a long-term, consistent time series of satellite observations, which allow the variability of the marine ecosystems to be studied on a global scale. The demand for (more or less) equally spaced datasets asks for AC processors which provide high coverage. If coverage claims the highest importance, processor approaches are to be preferred, which are not impaired by sun glint conditions. Although in the current status the focus lies on

phytoplankton-dominated clear waters (case 1), the processor which is best suited to facilitate seamless merging of different satellite sensors independent of the water types, will be preferred.

This algorithm development needs to balance two qualities of the processed dataset: on the one hand it should be as accurate as possible in deriving the geophysical products compared to quality controlled ground truth and on the other hand give the largest amount of valid data points in terms of completeness and consistency in space and time. While the match-up analysis focusses on the actual quality of the geophysical values, the methodology in this publication concentrates on matters of consistency and coverage.

In a preliminary study, the analysis of chlorophyll concentration maps derived from data from the Medium Resolution Imaging Spectrometer (MERIS) instrument, has revealed some artefacts in time series, when processed either with MERIS Ground Segment data processing prototype version 7.4 (MEGS 7.4, Antoine and Morel (2005)) or a neural network based regional processor approach (Doerffer & Peters, 2006). A strong signal was introduced in the time series analysis, which corresponded with the orbit repetition rate and the reoccurrence of a similar viewing and sun geometry after three days (in the North Sea). These systematic errors pointed towards unresolved angular dependencies in both atmospheric correction procedures (Müller, 2011).

In the course of the OC-CCI, time series of ECVs have to be produced that allow the meaningful interpretation of global trends. Any across-track dependence in normalised water leaving reflectances, which corresponds to systematic shifts at a single location, can hinder the assimilation of the data into ecosystem models, for example. This behaviour – independently from its actual source(s) – has to be characterised and if possible both addressed and resolved in the progress of algorithm development.

The products of four atmospheric correction processors with different underlying algorithms are assessed by tests in space and time on MERIS data. They employ those satellite data points that fall into rather large areas of interest over an entire year, instead of match-up data that is limited to isolated points in space. The tests assume that the quality of the retrieval is constant across track of the satellite sensor, if the algorithms proclaim their products to be valid.

These results complement the point-to-point match-up comparison (Müller & Krasemann, 2015; Müller et al., 2015).

The angular dependency tests intend to provide answers to the following typical questions:

- Does the algorithm, both atmospheric correction and normalisation, works on pixels affected by various sun glint conditions?
- Are there systematic or residual trends introduced by the processing?
- Are there any notable satellite sensor specific artefacts in the data after processing?

After an introduction to the MERIS instrument and the AC processors in this study, the methodology is presented and its results are discussed. It is proposed to combine the results by a semi-objective evaluation which leads to a ranking of the four processors.

2. Data processing for MERIS

2.1. The MERIS instrument

The MERIS sensor consists of five fixed cameras. Each one has been comprehensively spectrally characterised. The calibration effort leads to a radiometric model for each camera, which includes degradation effects and straylight correction. For each detector in the CCD array of the camera, the spectral behaviour is known allowing the development of algorithms that correct for small shifts in observed to nominal wavelengths (smile effect).

A MERIS scene of reduced resolution comprises of 1121 pixels across track. Each pixel has a geolocation Lon, Lat, a position across track X numbered from left to right. The number of track lines Y per scene varies according to the subset that is taken from a full orbit. The MERIS instrument comprises a camera system of five cameras with known spectral characteristics that all differ slightly. Cameras are counted from east (1) to west (5).

2.2. Atmospheric correction processors

The four atmospheric correction processors that have been chosen for this study have also been analysed in a match-up analysis (Müller et al., submitted for publication). The "POLYnomial based algorithm applied to MERIS" (POLYMER, Steinmetz, Deschamps, and Ramon (2011)) and the forward neural network (ForwardNN, based on Doerffer and Schiller (2007)), have been developed especially to derive water leaving reflectances even in sun glint conditions. To maximise consistency between products of and minimise biases in a merging procedure for different satellite sensors, the processor should ideally be applicable to observations from several sensors. The "SeaWiFS Data Analysis System" provides an interface to processing level 1 data to level 2 (l2gen, Feldman (2008)), which encompasses processing of "Moderate Resolution Imaging Spectroradiometer" (MODIS) and MERIS data as well as other ocean colour sensors. POLYMER and ForwardNN are able to handle SeaWifS and MODIS data. The MEGS processor is restricted to MERIS, but it represents the standard atmospheric correction procedure for MERIS level 2 products.

2.2.1. MEGS 8.0

This algorithm has been developed by Antoine and Morel (2011) for case 1 waters and has been extended to turbid waters by Moore and Lavender (2011).

The atmospheric correction for case 1 water is based on the assumption that the water leaving radiance in the near infrared spectral range at >700 nm is very low due to the high absorption by water and only the atmospheric contribution is observed. The MERIS spectral bands at 708, 753, 778 and 865 nm can then be used to determine the path radiance as well as its spectral shape. The path radiance is subtracted from the radiance at top of atmosphere (TOA) to get the water leaving radiance. The transmittance for the downward direction (sun zenith angle) and the upward direction (viewing zenith angle) is determined from the path radiance and used to determine the water leaving radiance.

The determination of the spectral shape of the path radiance is a critical step. It is determined by iteratively testing different aerosol types using, in addition, the spectral band at 560 nm.

In case of turbid water, the loop of the atmospheric correction is extended by including the water leaving radiances in the near infrared bands, determined by suspended particles with a fixed spectral shape. A detailed description of the MEGS atmospheric correction can be found in Antoine and Morel (2005, 1998, 1999) and Nobileau and Antoine (2005).

The MEGS processor in version 8.0 includes a vicarious adjustment performed with in-situ data collected at the MOBY and BOUSSOLE sites (Lerebourg, Mazeran, Huot, & Antoine, 2011).

A pixel is regarded valid if it has been identified as water with no clouds, ice haze or strong sun glint. If the product confidence flags (PCD) for reflectance (e.g. low sun angles, uncorrected glint, negative reflectances) or for the chlorophyll product algal_1 (e.g. atmospheric correction fails or there are difficulties with aerosol correction, uncorrected glint or whitecaps, high turbidity) are raised, the pixel is considered invalid (Table 1).

2.2.2. ForwardNN

This algorithm for the determination of water leaving reflectances from top of atmosphere radiances ("atmospheric correction"), the

Table 1
The combination of quality flags, which defines the validity of level 2 products, is given for each atmospheric correction processor. Satellite data is considered in the analysis, only if it fulfils the following quality criteria.

Processor	Valid L2 product defined by combination of individual quality flags
MEGS 8.0	NOT (land OR cloud OR ice haze OR high glint OR uncertain normalised surface reflectance OR aerosol model outside database)
ForwardNN	Sumsq < 10^{-5} and N.iter < 150
SeaDAS 6.3	NOT (land OR cloud OR sea ice OR high glint OR cloud shadow OR bright pixel OR aerosol max OR high solar zenith OR high sensor zenith OR navigation failure OR atmospheric correction warning OR atmospheric correction failure OR stray-light)
POLYMER	NOT (land OR cloud OR invalid L1 OR negative bb OR out of bounds)

retrieval of water optical properties and concentrations of water constituents, is based on an iterative optimisation procedure. Within this, the artificial neural networks (NN) are used as forward models. Examples of the NN inputs are the inherent optical properties of water and in-water constituents and the aerosol optical thickness, whereas the water leaving radiance reflectance spectrum or the TOA reflectances, are the outputs. In the iteration loop, the parameters of the forward models, i.e. the inputs of the NNs, are modified by an optimisation algorithm to achieve a best fit between the measured and computed spectrum.

The artificial neural networks are trained with a large simulated dataset of corresponding pairs of top of atmosphere (TOA) and water leaving radiance reflectances, ρ_w or pairs of ρ_w and IOPs respectively, which cover most of the possible conditions of atmosphere and water.

For this purpose, optical models were defined for atmosphere and water which cover different atmospheric properties; clear water of the open ocean with different phytoplankton pigment concentrations; and coastal waters with high concentrations of dissolved and suspended water constituents. Thus, water reflectances can be retrieved from the top of atmosphere reflectances over nearly all types of water.

The NNs used for the OC-CCI project simulate reflectances at 29 wavelengths. This covers the spectral range between 400 and 1020 nm and includes the spectral band sets of MERIS, MODIS, SeaWiFS and OLCI.

In the loop for fitting the observed spectra, the bands of interest can be selected according to the sensor and the importance of bands for a special type of water.

This version of the atmosphere model, which was used for generating the training dataset for the neural networks, included an erroneous angle definition in the part for computing the transmittances. We decided to keep the faulty version to demonstrate more clearly the strengths and limitations of processor comparisons. In match-up comparisons, which do not include sun glint conditions, this angular dependency does not affect the quality of the water leaving reflectances dramatically. But the effects can be clearly seen in the tests employed here.

The NN gives the sum of squared deviation between measured top of atmosphere reflectance and the modelled spectrum. A pixel is considered valid, if the sum of squares is smaller than 10^{-5} and less than 150 iterations were needed to achieve convergence. This criterion includes water, even with sun glint and semi-transparent clouds (Table 1).

2.2.3. l2gen 6.3

The default atmospheric correction used in the NASA SeaDAS software is described in a multi-sensor level 1 to level 2 code (l2gen). It reaches back to the approach devised for the Coast Zone Colour Scanner (CZCS, Gordon and Wang (1994)) and has been significantly updated over time. The code is developed and maintained by NASA's Ocean Biology Processing Group (OBPG) and in spring 2012 a version 6.3 is available. The software is designed to retrieve remote sensing reflectances directly from top-of-atmosphere radiances for a variety of space-borne sensors. In the standard atmospheric correction algorithm employed for NASA ocean colour (atmocor2), the TOA radiance is modelled taking into account 1) radiances from Rayleigh scattering by air molecules, 2) the scattering by aerosols, including multiple scattering interactions with the air molecules, 3) the contribution from surface whitecaps and foam, and 4) diffuse and direct transmittances and polarisation. The processor employs vicarious calibration with in-situ data from the Marine Optical Buoy (MOBY) (Franz, Bailey, Werdell, & McClain, 2007). The documentation (Franz, 2012) serves as a reference to the atmospheric correction algorithm employed in the software.

A pixel is valid, if it is identified as water and not influenced by clouds or cloud shadows, sun glint or algorithm failures (Table 1).

2.2.4. POLYMER 2.4.1

This algorithm has been developed by Steinmetz et al. (2011) for the atmospheric correction of MERIS imagery and is being extended to other sensors, including MODIS. It has been particularly designed to work in the presence of the specular reflection of the sun on the water surface, the sun glint. Atmospheric correction algorithms based on the estimation of the path radiance in near infrared bands usually do not work in these conditions, therefore Polymer leads to a vastly improved spatial coverage of the oceans. The algorithm is a spectral matching method over the whole available sensor spectrum. It uses two decoupled models: the water reflectance is modelled using two parameters — the chlorophyll concentration and the particles backscattering coefficient, and is mainly based on a semi-analytical model by Morel and Maritorena (2001). The reflectance of the atmosphere, including aerosols and a contamination by the sun glint, is modelled using a simple analytical expression, close to a polynomial, which is the sum of three spectral components of variable amplitude and of fixed spectral dependencies, namely power laws with respective exponents of 0, −1 and −4. The resulting model of the top of atmosphere (TOA) reflectance is therefore described by five parameters, which are optimised to reproduce the measurement in an iterative process using the Nelder–Mead algorithm (Nelder & Mead, 1965). Finally the above-water reflectances are obtained by subtracting the estimated reflectance of the atmosphere and sun glint from the TOA reflectances.

The current version 2.4.1 extends the algorithm description on several topics such as the cloud mask, implementation consideration and the estimation of error. Polymer was originally developed to process MERIS data, but it has been extended to process multiple sensors and is currently also applicable to MODIS and SeaWiFS.

Products are considered valid, if the pixel has not been identified as cloud or land and the backscattering coefficient does not become negative during the iterations or parameters take values out of bounds (Table 1).

2.3. A very short intercomparison of AC processor characteristics

The four AC processors show some differences in solving the task of transforming top of atmosphere radiances (MERIS level 1b) into water leaving reflectances. Table 2 gives an overview of major differences and common features.

In the course of an AC procedure, the first difference occurs in the application of a so-called smile correction. While POLYMER and ForwardNN use the actual wavelengths on a pixel by pixel basis (in look-up tables), MEGS utilises a linear spectral model for each camera, which builds on the pixel by pixel characterisation. The l2gen processing includes a smile correction for MERIS data, which is based on the same model as MEGS.

While POLYMER and ForwardNN do not consider a vicarious adjustment, MEGS and l2gen apply their individual sets of gain coefficients to each MERIS band. They are applied to TOA reflectances for MEGS (Lerebourg et al., 2011), whereas l2gen modifies the TOA radiances (Franz et al., 2007). The gain factors for each band are the product of the combination of satellite sensor, in-situ measurements and AC procedure. It is their aim to reproduce the in-situ measured water leaving radiances accurately by applying a set of factors to the TOA radiances and

Table 2
Comparison of atmospheric correction procedures. Each processor consists of several modules which use their specific algorithms to address necessary corrections or modelling aspects. This is an overview of the angle dependent processes, more details are given in Section 2.3.

Features	MEGS	POLYMER	ForwardNN	l2gen
Smile correction	Linear model	Pixel-by-pixel	Pixel-by-pixel	Same as MEGS
Vicarious adjustment	TOA reflectance (MOBY, BOUSSOLE)	–	–	TOA radiance (MOBY)
Sun glint handling	Masked out	Corrected	Corrected	Masked out
Polarisation	Included in Rayleigh scattering model	–	(Optional)	Included in Rayleigh scattering model
Basic principle	Correction for NIR in-water contribution	Spectral optimisation 5 param.	Spectral optimisation 8 param.	Correction for NIR in-water contribution
Normalisation	Based on Morel and Genetili (1996), (in ODESA)	Based on Morel and Genetili (1996),	NN model approach	Based on Morel and Genetili (1996),

processing them with the AC. The MEGS approach uses in-situ data from MOBY and BOUSSOLE, whereas l2gen calculations are based on MOBY alone. Although these considerations are more important in a study which involves in-situ measurements, the vicarious adjustment can be responsible for overall shifts in values of derived geophysical fields.

It would be out of the scope of this paper to cover in detail all the in-depth differences in the algorithms and models involved in the ACs. Assuming that the across-track methods visualise angular dependent processes and their artefacts in the first place, differences in the atmosphere model approaches might be the cause of the strongest effects. At least in this case study it is known that during modelling the transmission coefficient for the ForwardNN training, an error in the angle conversion occurred. While the severity of this issue is not obvious in the match-up analysis, it cannot be denied when looking at a satellite scene (Fig. 1).

Although sun glint is identified and modelled in MEGS and l2gen, both are not equipped to correct for the specular sun reflection and identified pixels are masked out. POLYMER and ForwardNN incorporate a sun glint contribution in their reflectance models and derive water leaving reflectances in this condition. Therefore it is to be expected that POLYMER and ForwardNN allow for a much larger coverage of data.

Polarisation effects are included in the Rayleigh molecule scattering model of l2gen and MEGS, whereas the ForwardNN includes these effects optionally (not here). Atmospheric models in POLYMER do not account for polarisation.

The basic principle behind MEGS and l2gen is the assumption that the contribution of water leaving radiance in the near-infrared is negligible (black pixel assumption) and any radiance is dominated by the atmospheric processes. After deriving (or choosing) an appropriate
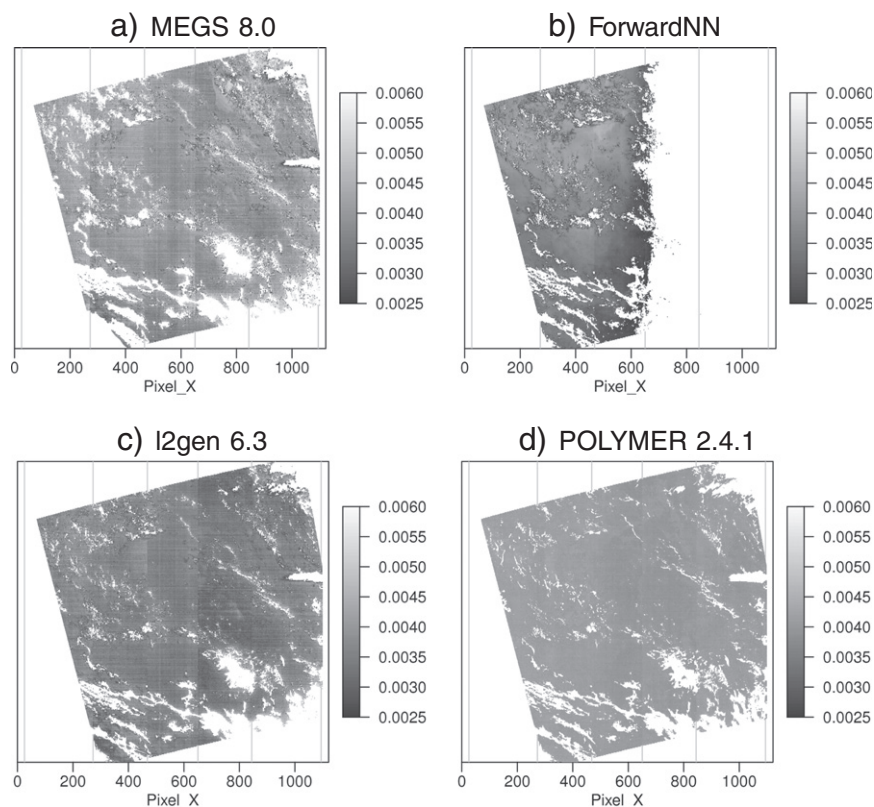

Fig. 1. Extraction of a MERIS scene covering the South Pacific Gyre (definition see Section 2.5), April 10th 2008. Normalised water leaving reflectance ρ_{wn} at 560 nm derived by four atmospheric correction processors. MERIS cameras are counted from right to left and their extents are indicated by vertical lines. The retrieval of the ForwardNN processor fails in camera 1 and partly in 2. POLYMER exhibits less variance than the other processors. Camera boundaries can be found in the MEGS and l2gen products, including a lower mean value in camera 2 for l2gen products.

aerosol model based on the NIR data, their spectral behaviour is extrapolated to the visible spectrum. In POLYMER and ForwardNN, the shape of the entire spectrum is fitted simultaneously in an iterative spectral optimisation process.

2.4. Data processing

The data processing starts with running the four atmospheric correction processors in their current versions (Spring 2012). The water leaving reflectances have to be fully normalised, which turns the reflectances influenced by the bidirectional radiative transfer characteristics into (ideally) angle independent values. The sun and view angle dependent measurements are transformed to an angle independent geometry with the sun position at the zenith and the viewing direction in the nadir. While three processors include normalisation procedures, which follow the approach of Morel and Gentili (1996), the neural net algorithm uses a specially trained network for this task. In order to fully normalise the MEGS processed data, the implementation within the Optical Data processor of the European Space Agency (ODESA) is used.

In a scene covering the area of interest, all valid pixels are selected according to each processor's individual quality flags (Table 1). The selection of pixels is expected to differ from processor to processor (Fig. 1). While the POLYMER water leaving reflectance at 560 nm has a rather low variance (median and standard deviation: $4.1 \pm 0.12 \cdot 10^{-3}$), the high variance in the MEGS product originates in extremely high and low values in the presence of undetected clouds and cloud shadows ($4.1 \pm 0.55 \cdot 10^{-3}$). l2gen and ForwardNN lead to lower mean values (ForwardNN: $3.5 \pm 0.64 \cdot 10^{-3}$, l2gen: $3.6 \pm 0.36 \cdot 10^{-3}$). Both MEGS and l2gen show a systematic difference between cameras, which are observable in camera boundaries and a lower mean value in camera 2 for the l2gen product.

The valid pixels build the baseline of the angular dependency tests, which focus on three products: the fully normalised water leaving reflectance ρ_{wn} at 443 nm (chlorophyll absorption maximum) and 560 nm (chlorophyll absorption minimum) and the chlorophyll concentration as a proxy for a combination of wavelengths. The results shown here concentrate on the water leaving reflectances in the South Pacific Gyre region.

2.5. Definitions and area of interest

The area of the South Pacific Gyre (SPG, 23.5–32°S, 129–139°W) has been chosen for its very oligotrophic conditions and is expected to have minimum reflectance in the NIR, thus the 'black pixel assumption' should hold. The dataset consists of 349 L1B MERIS scenes (third reprocessing) from January until December 2008. In order to assess the behaviour at higher latitudes and lower sun elevation, a second area in the North Atlantic has been selected (NA, 50–60°N, 25–40°W). Due to cloudiness during autumn and winter the dataset has been restricted to the period from March to August 2008 (290 MERIS scenes). Both sites are considered case 1 water and rather large, spatially homogeneous areas with no strong spatial features.

The proposed methodology is demonstrated in the SPG region. The area has the advantage that it exhibits mainly random, scattered cloud cover throughout the year, while the NA area typically suffers from larger and seasonally dependent cloud cover. Therefore, results can be interpreted more easily in the SPG region, where randomness of data loss in satellite scenes can be balanced by all statistical methods which include some kind of averaging technique. In the following section, each method is defined and its results visualised and discussed.

Most of the following methods employ statistics based on the cross track position of pixels, in order to quantify their trends.

3. Methods and results

3.1. Estimating MERIS residual cross-track effects

3.1.1. Mean per cross track pixel over the entire period

For each product; e.g. normalised water leaving reflectances $\rho_{wn}(\lambda)$ at wavelength λ, the mean over the entire period of time t for each cross track pixel X and all scenes is calculated regardless of their specific geolocation.

$$\overline{\rho_{wn}}(X, \lambda) = \frac{1}{N(X)} \sum_Y \sum_t \rho_{wn}(X, \lambda)_{Y,t} \qquad (1)$$

It is expected that the product of an ideal processor shows no across-track trends. Minor random inhomogeneities in the water leaving reflectance should have cancelled each other out over time and observed space. The different discrete orbit paths cover the region of interest to a predetermined percentage and with varying but fixed viewing angles and continuous sun angles according to the overpass time and the seasonal variation of the sun elevation. These angular dependencies should have been resolved by the normalisation procedure. In the ideal case only a flat line would remain. Thus, it can be argued that all visible trends and shifts are associated with unresolved spectral characteristics of the distinct cameras of the spectrometer if they are similar for processors, which employ the same smile correction.

In order to check for a temporal dependence, the mean value is calculated for each month separately. This signal can be expected to show a seasonal cycle, which corresponds to the changing biology during the year. Also effects of sun glint influence on the different procedures may become more pronounced in monthly resolution.

3.1.2. Results

The number of valid pixels differs strongly across track between the sun glint masking algorithms (MEGS and l2gen) and the POLYMER algorithm, which is designed to work in such conditions (Fig. 2). The known erroneous behaviour of the ForwardNN leads to almost no valid pixels on the eastern side of the scenes. Only POLYMER shows almost no trend in water leaving reflectances. The flatness of the $\overline{\rho_{wn}}(443$ nm) originates in the special purpose of this wavelength in the minimisation process of spectral matching. Vertical striping is evident in the noisy structures in the MEGS and l2gen processing at 560 nm. With spikes at the same pixel positions it can be argued that the non-random parts of the cross-track effects can be corrected more efficiently by employing the pixel-by-pixel smile correction which is used in the ForwardNN and POLYMER processing and yields a visible advantage in terms of smoothness. Camera boundaries are evident in several products and processors. Overall POLYMER is the least affected, except for the sun glint area observed with cameras 1 and 2 (pixel 650 to 1121). The products of the ForwardNN are potentially as well behaved as POLYMER's in terms of smoothness and small discontinuities at camera boundaries, but the drop in valid pixels does not allow a meaningful interpretation of the statistics in cameras 1 and 2. The POLYMER flags might even be a bit too relaxed, as they identify more valid pixels towards the sun glint area of a scene (camera 2) than on average (almost constant in cameras 1, 3, 4).

MEGS and l2gen show similar trends in each camera. Influences from all angle dependent processes, which cannot be distinguished, might add to this systematic behaviour and result in the observed contrasting slopes.

If the cross track mean of the $\rho_{wn}(560$ nm) is resolved per month, some further insights can be gained (Fig. 3). Large noise in months with sun glint conditions (southern summer) may either arise from the very low amount of valid pixel or the residual effects of the sun glint itself. For cameras 3 to 5 the ForwardNN and POLYMER ρ_{wn} are rather smooth (little pixel-by-pixel noise), camera boundary effects
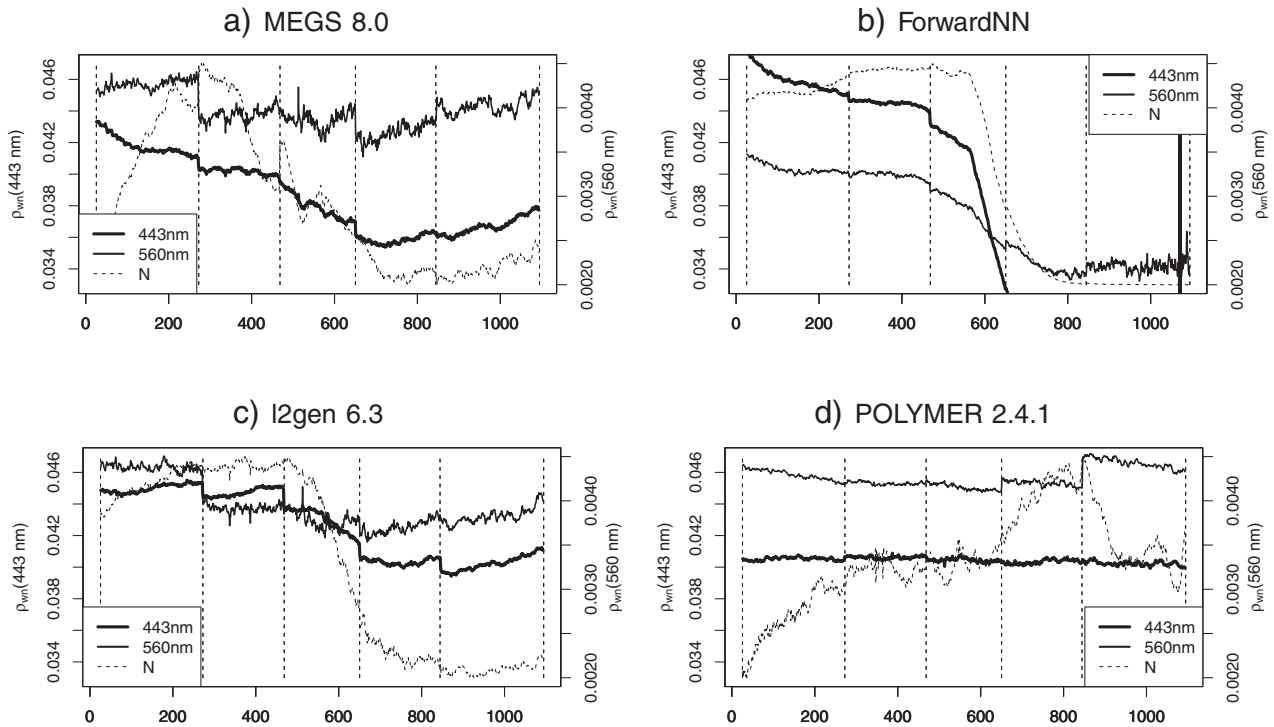
Fig. 2. Mean per cross track pixel and entire period for ρ_{wn} of four AC processors in the SPG area. Line thickness represents ρ_{wn} at 443 nm and 560 nm and number of pixels (dotted). The number of valid pixel ranges from MEGS: $(15 - 29) \cdot 10^3$, ForwardNN: $10 - 51 \cdot 10^3$, l2gen $(18 - 43) \cdot 10^3$, POLYMER $(34 - 45) \cdot 10^3$. Vertical dotted lines represent MERIS camera boundaries. The cameras are counted from right (1) to the left (5).

are small and the relationship between offsets of different months is rather constant. This behaviour can be explained by their similar approach to correct for shifts in the actual wavelength on a pixel by pixel basis (smile correction). In sun glint conditions the camera boundaries at cameras 1/2 and 2/3 increase strongly, with a positive correlation between the strength of sun glint conditions and the height of the reflectance offset (see POLYMER, camera 1). The remaining noise in the POLYMER mean reflectance shows systematic tendencies, with similar shapes of maxima and minima at the pixel positions, which may arise from residual instrument calibration issues in the smile correction. Interestingly the l2gen product exhibits a change in sign of the offset with respect to the May data, which is the most stable across track. The effect correlates with the intensity of the sun glint. Effects at camera boundaries are particularly strong between cameras 4 and 5. The effects seen in the MEGS product are rather large offsets between camera 4 and 5 and complex structures per month and camera. Part of the noisiness may be explained by the different smile correction approach, which uses a linear fit instead of the nominal wavelengths for each pixel (Table 2).

3.2. Time series of coverage

3.2.1. Spatial asymmetry test

With the results of the mean per cross track pixel in mind, it becomes evident, that any time series on a daily basis at a single location might suffer strongly from the across-track trends. A systematic signal is introduced, which depends on the orbit position and therefore which camera (or even detector within) is responsible for the observation. Data points of a time series might come from camera 5 on one day and from camera 1 on the next, which would obviously create a signal which is not related with any process in the water (see also Section 3.3, Fig. 5).

In the mean value of a regional subset, which is smaller than the width of a swath, the influence of the trend can still be found. As long as clouds can be considered equally distributed, they will not introduce a systematic signal in an spatial mean value, although they can reduce the amount of data considerably. In addition, most AC processors use angle dependent criteria to mask or identify sun glint conditions, which are situated in the eastern half of the scene (for MERIS).

The spatial asymmetry test counts the amount of pixels originating from the left or right side of a scene. The across-track pixel index X is counted negatively from the centre line at 1121/2 and positively from the centre line to the right. The centre of mass α of valid pixels (amount N) is calculated relative the centre of the scene at time t.

$$\alpha(t) = \frac{1}{N(t)} \sum_{i=1}^{N(t)} \left(X_i(t) - \frac{1121}{2} \right) \qquad (2)$$

Due to the discrete orbit paths, the amount of available data depends on the coverage of the area by the individual swath. Even in the ideal case of all pixels in each scene being valid, the pattern of coverage driven by the discrete orbits is to be expected.

3.2.2. Results

The orbit pattern is more or less visible for all processors (Fig. 4). The more pronounced it appears, the closer the distribution of pixels is to ideal coverage. Masking effects by randomly scattered clouds or otherwise missing data are low. Due to sun glint conditions, pixels on the right hand side of the scene have been omitted; moving those scenes to negative spatial asymmetry or omitting some scenes entirely (e.g. MEGS, l2gen). The ForwardNN quality flags reject almost all pixels on the right side of the scene (Fig. 2b), which corresponds with the known error in the atmosphere modelling. While for the other
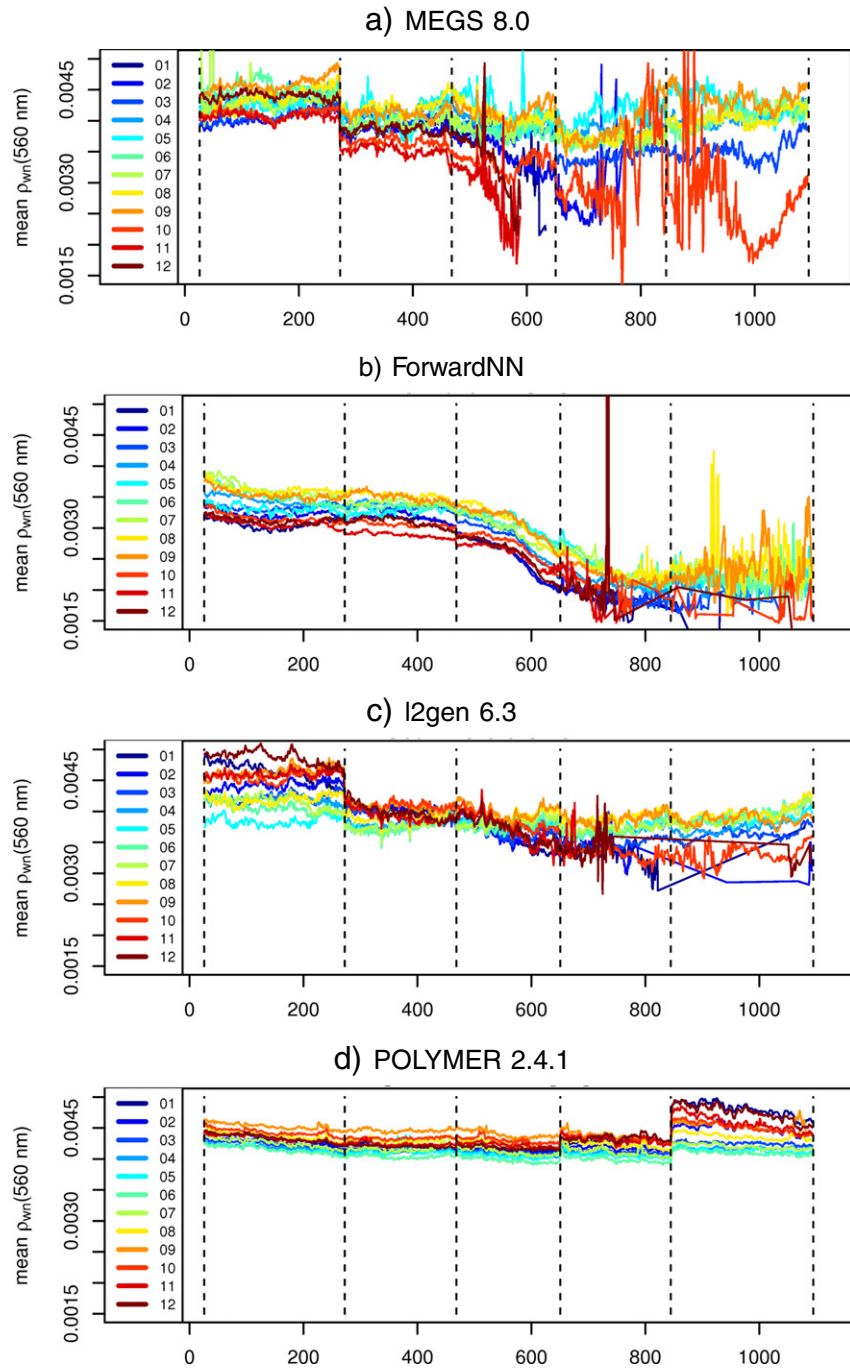
Fig. 3. Monthly mean per cross track pixel for $\rho_{wn}(560 \text{ nm})$ of four AC processors in the SPG area. The colour represents the month, the vertical dashed lines represent camera boundaries.

processors, the highest amount of valid pixels always occurs with an equal distribution of pixels to the east and the west of the nadir line, the ForwardNN data is clearly shifted to the west. POLYMER displays the proposed ideal data coverage over the entire year. The quality flags suggest that the algorithm works fine in sun glint conditions. The coverage is of course no guarantee for precise geophysical values. The MEGS processing excludes more pixels than l2gen, which leads to the stronger random scattering in the distribution. The applied quality flags for MEGS may be more restrictive than for l2gen.

The stronger the asymmetry, the more contorted the spatial mean value for a time series will be, especially due to the across-track trend (if present in the processing) and secondly due to the limited amount of data and coverage of the region.

3.3. Biases on sensor level

3.3.1. Time series per camera

The mean per cross track pixel (Section 3.1) has revealed rather strong systematic shifts or trends per camera. Calculating the time series
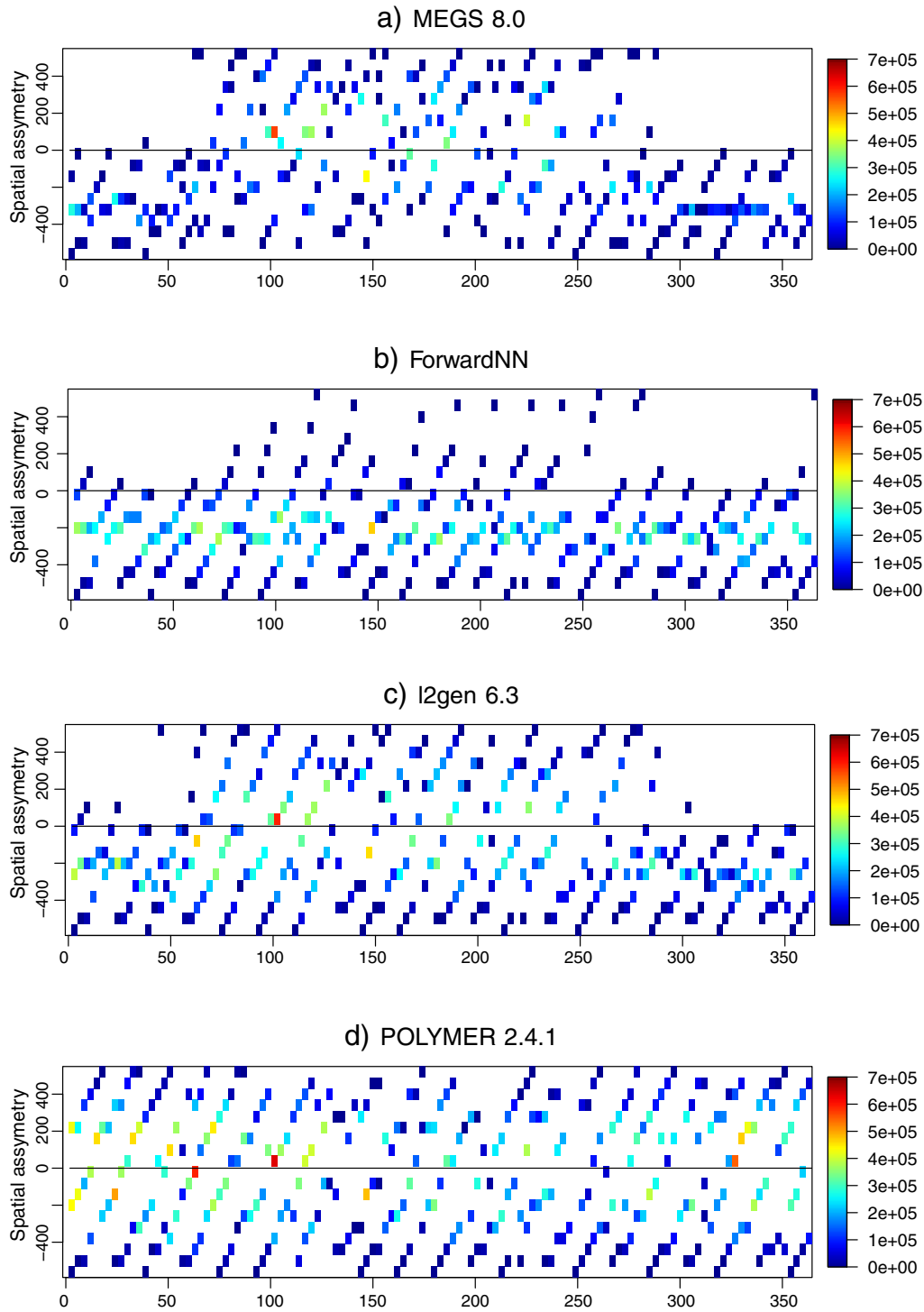
Fig. 4. Time series of coverage and spatial centre of mass relative to the nadir line calculated from all valid pixels per scene. The x-coordinate states the day of the year. The colour corresponds to the number of valid pixels inside each scene, which covers the SPG region. Scattering in the pattern accounts for patchiness (e.g. clouds, sun glint, other effects) in valid data, while the pattern itself emerges from the discrete orbit paths of MERIS.

per camera and comparing it with the overall mean strives to resolve this behaviour in time.

For each of the five cameras which build the spectrometry system of MERIS, the time series of water leaving reflectance $\overline{\rho_{wn}}(t, cam)$ is computed separately. All valid data per scene is taken into account. The deviation $\Delta_{cam}(t)$ of the average per camera from an overall average of all

valid pixels (Eq. (5)), $\overline{\rho_{wn}}(t)$ is interpreted as the influence of camera specific trends and biases on the products.

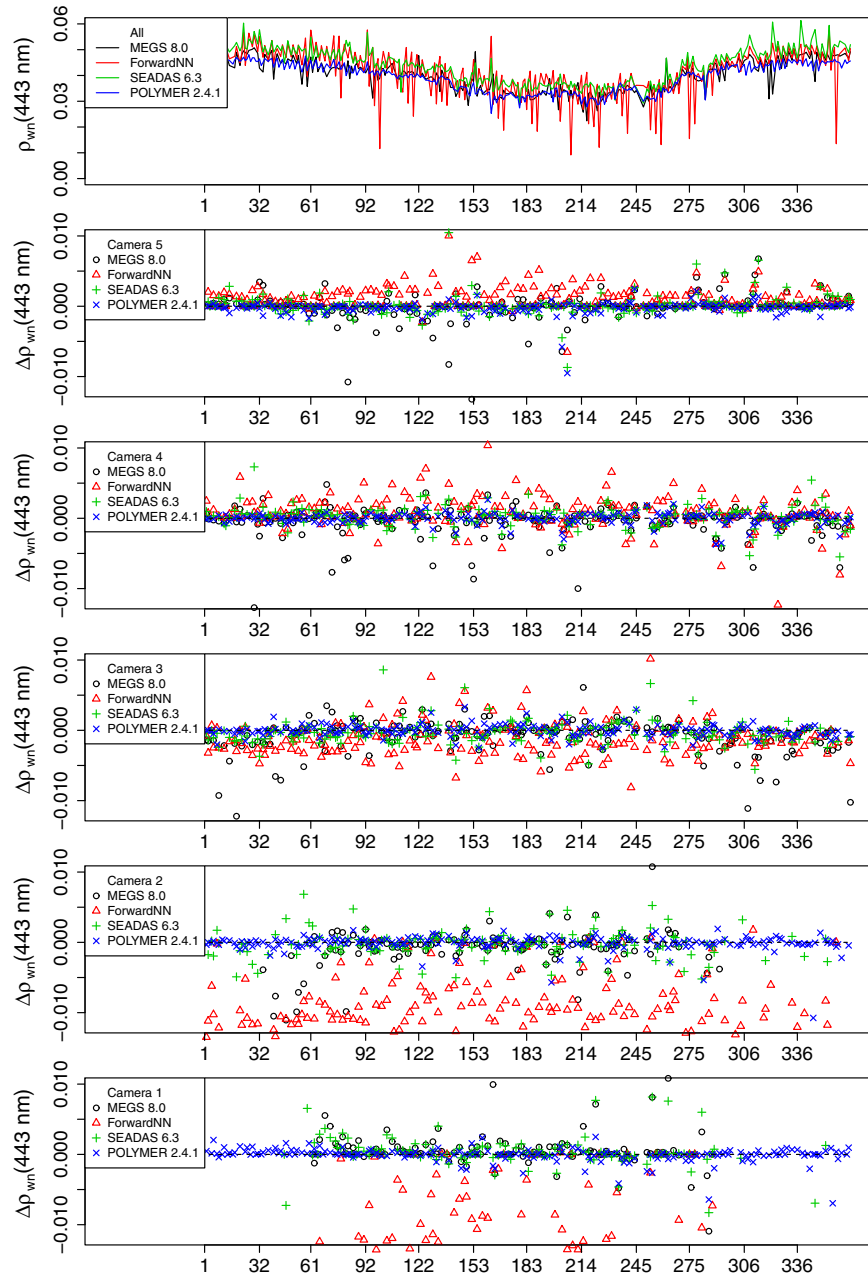$$\overline{\rho_{wn}}(t) = \frac{1}{N}\sum_{X,Y}\rho_{wn}(t)_{X,Y} \qquad (3)$$

Fig. 5. Time series of deviations between mean per camera and average over the entire scene for ρ_{wn} at 443 nm in the region of South Pacific Gyre. The cameras are counted from east (1) to west (5). Strong systematic deviations are evident for the ForwardNN products due to the known error in transmission modelling.

$$\overline{\rho_{wn}}(t, cam) = \frac{1}{N_{cam}} \sum_{X,Y} \rho_{wn}(t, cam)_{X,Y} \qquad (4)$$

$$\Delta_{cam}(t) = \overline{\rho_{wn}}(t, cam) - \overline{\rho_{wn}}(t) \qquad (5)$$

The amount of data points for the column mean is expected to be lower in the right hand side columns for those algorithms which exclude the sun glint conditions.

3.3.2. Results

The time series of reflectances at 443 nm exhibit the same seasonal pattern independent of the processor (Fig. 5, upper panel). The deviation of the average from a single camera to the total average is close to zero for POLYMER and reveals only little scatter, simply reflecting the flatness

of the mean response over the entire track (Fig. 2d). The ForwardNN deviations denote the other extreme. They scatter strongly and display large biases for the different cameras, which are to be expected due to the trend (Fig. 2b). The camera dependent deviation calculated from MEGS products shows more scattering than the l2gen results, which is not surprising given the stronger trends in MEGS than l2gen (Fig. 2a, c). Particularly towards the beginning and end of the year, valid pixels get scarcer due to increasing sun glint conditions in the southern summer, therefore increasing scatter (see colouring in Fig. 4a, c). The scatter may also originate in unidentified sun glint conditions which are not corrected (or excluded) properly in MEGS (see especially camera 2, $\rho_{wn}(443 \text{ nm})$, day 30 to 70 and camera 3, $\rho_{wn}(443 \text{ nm})$, day 1 to 60 and 300 to 365).

The time series of water leaving reflectances at 560 nm exhibit no visible seasonal pattern independent of the processor (Fig. 6). Reflectances processed by MEGS and l2gen coincide more or less. This
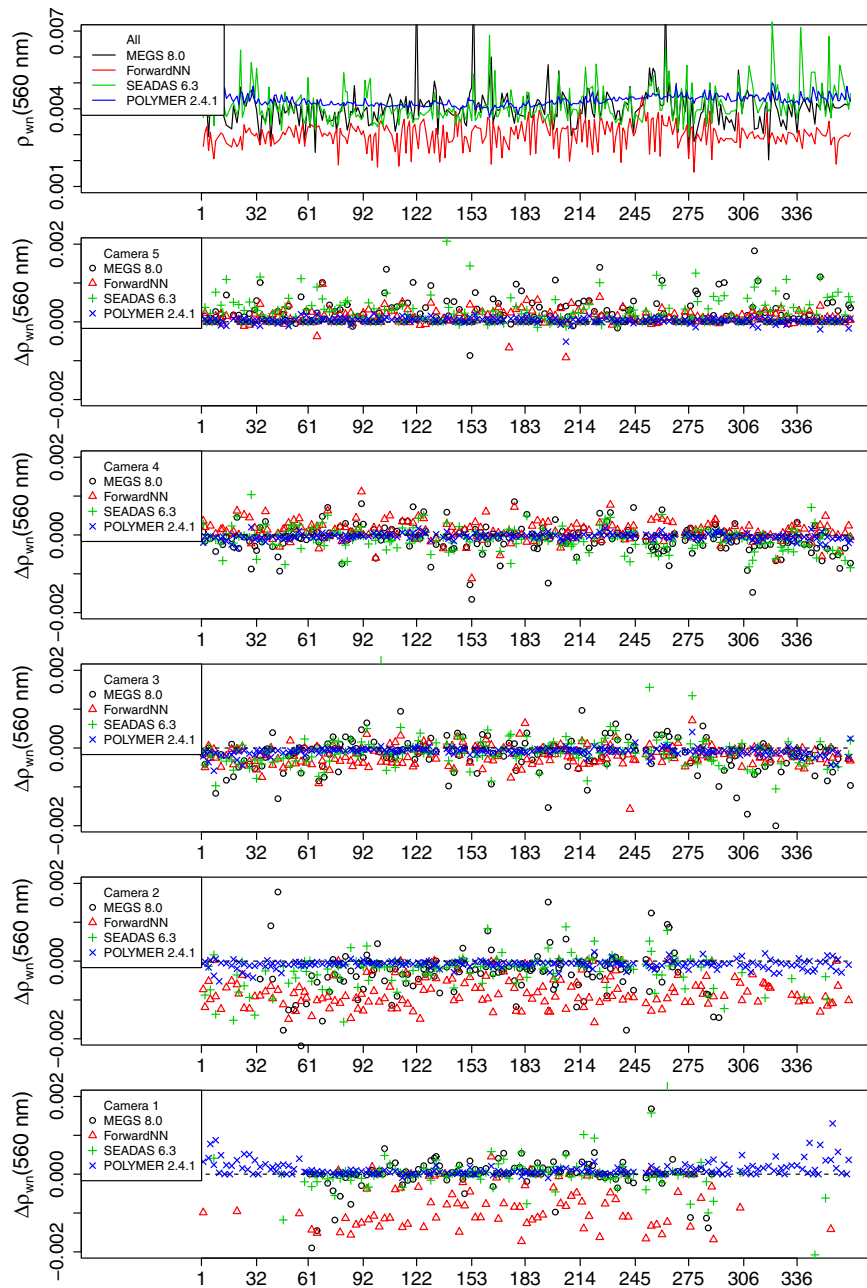
Fig. 6. Time series of deviations between mean per camera and average over entire scene for ρ_{wn} at 560 nm in the region of South Pacific Gyre. The cameras are counted from east (1) to west (5). Strong systematic deviations are evident for the ForwardNN products due to the known error in transmission modelling. In the sun glint affected parts (camera 1 and 2) in the southern summer POLYMER reveals a slight degradation of product quality.

agreement of the products can arise from the vicarious adjustment, which both processors employ. Values of products from POLYMER (dashed and dotted) are slightly higher with less scatter, while products from ForwardNN are generally lower.

The deviations of a single camera mean to the overall mean value show biases according to the known trends (Fig. 2). The scattering in the POLYMER reflectances increases in the southern summer in camera 1 and 2, which observe the sun glint affected areas. This deviation from the otherwise low and featureless differences hints towards a slight degradation of the products' quality due to the glint influence. In comparison with the other processors, POLYMER provides the most stable products throughout the year. Apart from the POLYMER products, the remaining processors give

similar results in terms of scatter per camera, although the MEGS products appear a bit noisier than l2gen and ForwardNN products in cameras 3 to 5. The strong bias of the ForwardNN products in camera 1 and 2 originates in the known error in atmosphere modelling.

At both wavelengths, the time series includes signals at high frequencies. In the (erroneous) ForwardNN product, this signal is the most pronounced. However, it can also be identified in the products of the other processors. The stronger the trend across track, the more pronounced these signals are. They follow the harmonics of the orbit repetition cycle of 35 days. E.g. after 3.18 days the observation geometry and across track coverage are most similar to a given reference, and therefore so are the mean values.

3.4. Residual cross-track effects of smile correction and normalisation

3.4.1. Relative mean per cross track pixel and period

Whereas the mean per cross track pixel (Section 3.1) provides absolute values of the artefacts across track, the relative mean allows direct comparison of the different products trends. This method emphasizes the trends while the influence of the biases is reduced.

This method is based on a level 2 to level 3 comparison, which has been developed to "...quantify and track changes in residual cross-scan artefacts and [...] detector-to-detector relative differences." (see http:// oceancolor.gsfc.nasa.gov/DOCS/methods/sensor_analysis_methods.html, section VII).

In a first step, level 3 products are created which average 15-days of data on a coarse latitude and longitude grid of approx. 9 by 9 km resolution, $\overline{\rho_{wn15}}(t, Lon, Lat)$. Each of these grid pixels comprises data from a variety of sun and viewing angles so that random and systematic angular effects should cancel out, which have not been eliminated through normalisation. Only grid pixels with more than 20 data points are taken into account. The 15-days mean is treated as the reference value for the level 2 data at the centre of the period. All pairs of valid level 2 pixels (with original resolution of MERIS) and their collocated level 3 counterparts are gathered for each pixel number X. The ratios of level 2 to level 3 pixels for a single MERIS reduced resolution pixel position X are averaged, providing a mean relative error $\overline{\rho_{wnrel}}$.

$$\overline{\rho_{wnrel}}(X) = \frac{1}{N_X} \sum_t \sum_Y \frac{\rho_{wn}(X, t, Lon, Lat)_Y}{\overline{\rho_{wn15,t}}(t, Lon, Lat)} \qquad (6)$$

To check for temporal dependencies, the relative error is also calculated on a monthly basis.

3.4.2. Results

The total amount of valid pixels is almost constant over the entire swath for POLYMER (Fig. 7, bottom), whereas the drop in pixel numbers occurs due to exclusion of sun glint conditions on the eastern part of the scene for the other processors. In the western part, all algorithms provide more valid data points than MEGS.

If no residual effects were present, the relative mean would be 1. In the blue, the relative error ranges from −2% to 1.5% excluding the ForwardNN products (Fig. 7, top). POLYMER's behaviour is less affected by the camera system than l2gen and MEGS (and ForwardNN), which show trends and clearly cut camera boundaries at 443 nm. The smile correction seems to be working best in the POLYMER algorithm. l2gen and MEGS show similar behaviour in terms of in-camera trends and discontinuities at camera boundaries, as can be expected at least partially by using the same smile correction model.

Relative errors at 560 nm range between 7% (Fig. 7, middle). Except for camera 1 (first on the right), the POLYMER processing promises more stability than any other algorithm. Even in the area affected by sun glint (mostly camera 2), the relative error remains low for POLYMER products despite, to some extent, their quality degrading according to occurring trends and strong discontinuities at camera boundaries.

The monthly relative errors (Fig. 8) are affected by the seasonality, but the effects appear to be rather random and with a large noise signal in the MEGS and l2gen products. A detailed analysis of the temporal
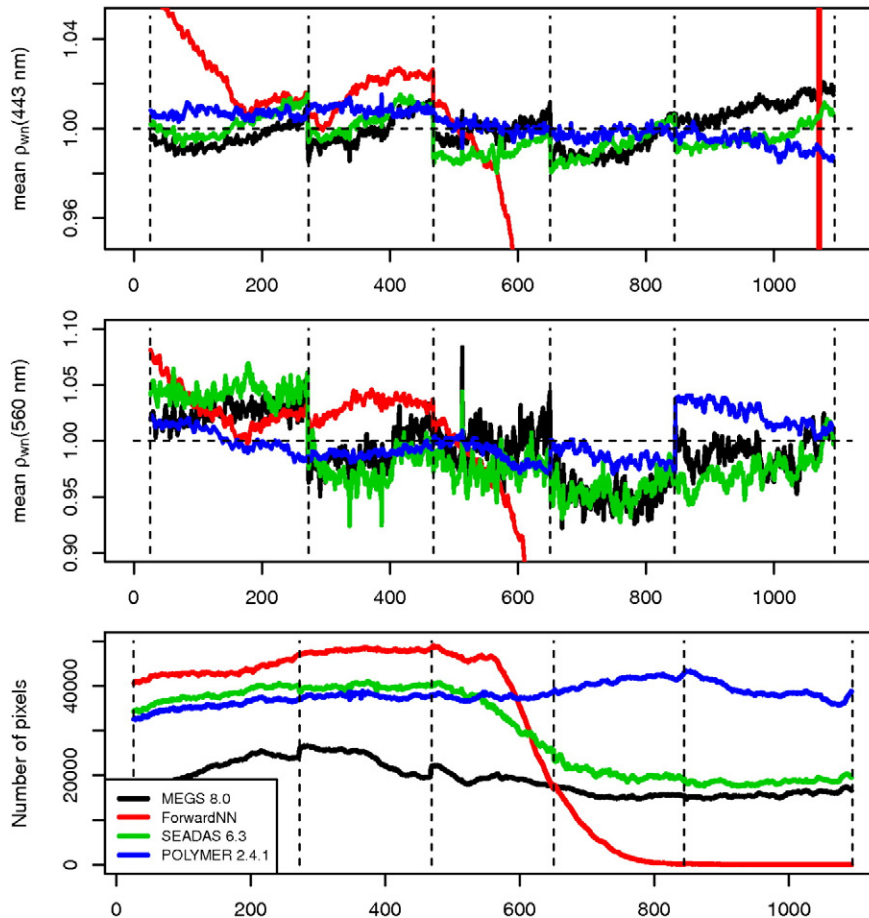

Fig. 7. Relative mean per cross track pixel, level 2 to level 3 comparison over SPG for normalised water leaving reflectances at 443 nm and 560 nm. Vertical dotted lines mark camera boundaries in the MERIS system, cameras are counted from right (1) to left (5).
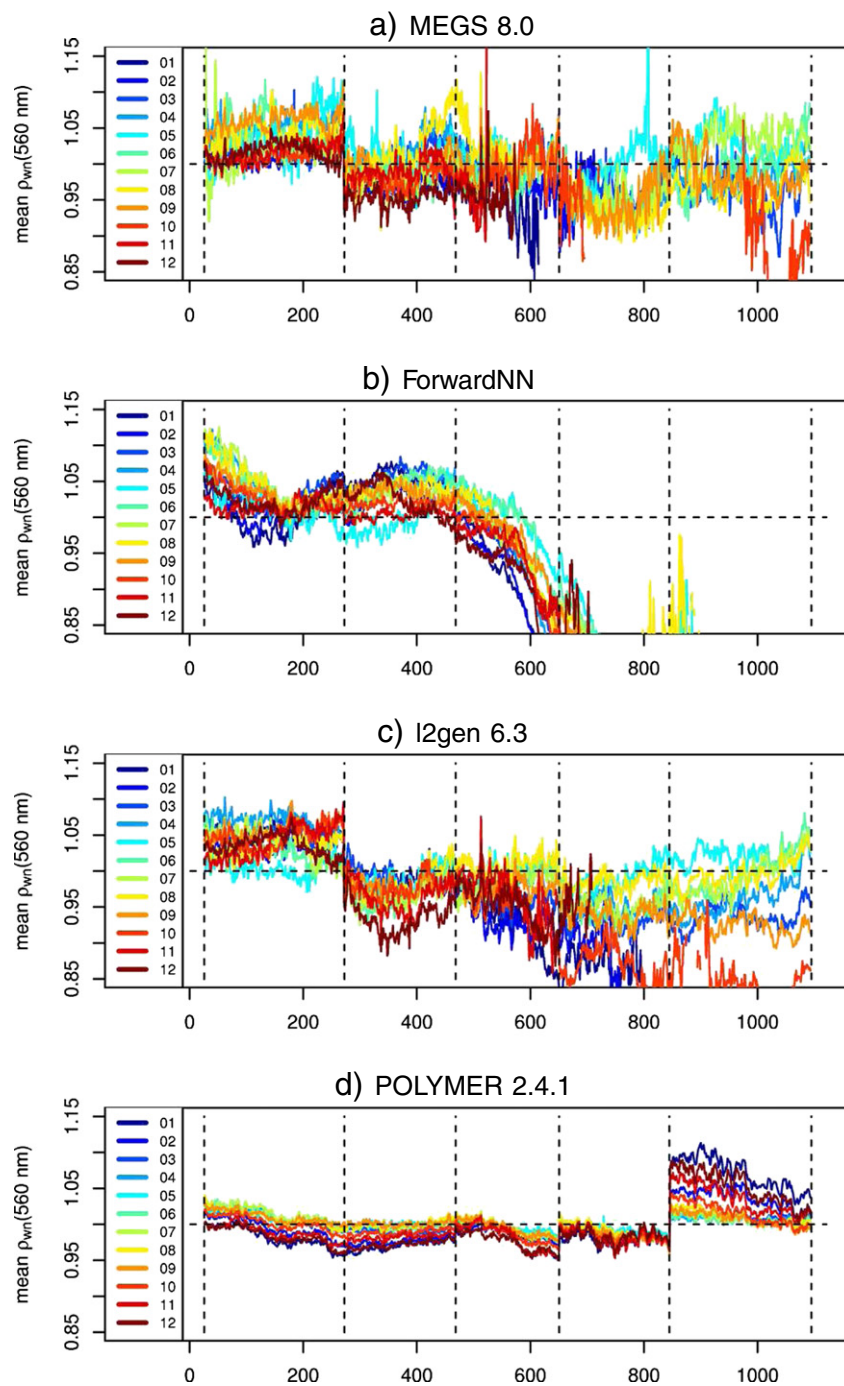
Fig. 8. Monthly relative mean per cross track pixel for $\rho_{wn}(560 \ nm)$ of four AC processors in the SPG area. The colour represents the month, the vertical dashed lines represent camera boundaries.

signal, which corresponds to different (mean) illumination conditions during the observation, is out of the scope of this paper. The relative error of the POLYMER products is quite stable over time and the four cameras 2–5, whereas a strong seasonal signal is superimposed on the error in data of camera 1. This again suggests, that POLYMER either declares too many pixels in the sun glint area as valid, which increases the variability with viewing geometry drastically and leads to the positive correlation between relative error and amount of sun glint pixel.

4. Discussion

Instead of evaluating each method independently, it seems more logical to combine the findings of all methods that address the same

Table 3
Summary of the test results converted into scores for the SPG dataset and the four atmospheric corrections.

Test/algorithm	MEGS 8.0	ForwardNN	l2gen 6.3	POLYMER 2.4.1
No discontinuities?	1.5	(3.5)	1.5	3.5
No trends per camera?	2	(1)	3	4
No bias per camera?	2	(1)	3	4
Temporal stability?	2	(2)	2	4
Coverage?	2	(1)	3	4
No noise?	1	(3.5)	2	3.5
$\sum$	10.5	12	14.5	23

product characteristics. The following six characteristics have a major influence on any further analysis of the dataset and their behaviour can be assessed within the methodology (Table 3):

1. Discontinuities between cameras are most prominent in the MEGS and l2gen processing and are much weaker but comparable in the ForwardNN and POLYMER products (methods 1 and 4). The smile correction of the later seems to work more efficiently than the MEGS approach.
2. Trends per camera are clearly the weakest in the POLYMER products and increase for l2gen, MEGS and ForwardNN products (methods 1 and 4). The last rank has been assigned to ForwardNN due to its relative error shown in method 4. Whether any part of the atmospheric correction or normalisation is the main source of the observed effects cannot be concluded without further investigation.
3. Systematic offsets per camera are clearly strongest in the ForwardNN products and decrease for MEGS, l2gen and POLYMER products respectively (methods 1 and 3), disregarding that the true value is unknown. Differences may be caused by the influence of unresolved spectral characteristics, which are not covered in the instrument radiometric model or the spectral model of the smile correction. As all AC processors are applied to level 1 data which has been processed with the same spectral calibration models, it is unlikely, that the major patterns in the artefacts originate within the instrument calibration.
4. Temporal stability can easily be assessed by the monthly characteristics and the inspection of the time series. Most products are affected negatively by the sun glint condition, whether they actually correct for these conditions or not. MEGS products are quite stable, which means that the masking of sun glint conditions is very effective. POLYMER derives clearly the most stable products, though a time dependent offset has to be expected in data of camera 1.
5. Coverage is very high for POLYMER, almost as regular for l2gen products which exclude sun glint areas, good for MEGS and not very satisfactory for ForwardNN products due to the error (methods 2, 1 and 4). Taking temporal stability (and results from in-situ comparisons) into account, the POLYMER products offer a good basis for time series analysis. It seems advisable to exclude data from camera 1 in glint conditions to trade stability off against coverage. Nevertheless extensive coverage is desired and a huge advantage, if time series of both high temporal and spatial resolution are considered.
6. Noise, or more explicit vertical striping, is quite strong in the MEGS products, less prominent in the l2gen products and equally well treated and reduced in ForwardNN and POLYMER (methods 1 and 3). The combination of the spectral fitting methodology and the pixel-by-pixel smile correction can be responsible for the noise reduction compared to MEGS.

In order to summarise the results of the different tests, a ranking system is proposed. These subjective scores are based on visual inspections of the test results and follow the goal of identifying the processor, enabling us to create a consistent time series with high temporal and spatial coverage. The appointed scores adhere to the following ranking scale; 4 points being for the best performing algorithm, 1 point being for the least performing algorithm. If the choice is undecided, the products are appointed the same rank. The sum of ranks is normalised to give a total of ten per criterion. To our judgement, POLYMER is in the lead, followed by l2gen and ForwardNN and MEGS (Table 3).

5. Conclusion

Four angular dependency tests have been introduced and applied to the MERIS data which has been processed with four different atmospheric correction processors at two selected regions. Their results allow a comprehensive insight into the processor and satellite sensor behaviour, which cannot be assessed with a point-by-point match-up comparison. For example, the failure of the ForwardNN in the eastern half of the scene has not become obvious in the match-up point comparison. Most match-up points are covered by data from cameras 3–5, especially if a common set of valid data points is selected and sun glint cases are therefore excluded.

The sources of the described effects are difficult to separate and may include sensor specific reasons such as residuals from the instrument calibration concerning straylight and the radiometric models. Or they may originate with at least one of the variety of model assumptions and their respective implementations which are used in the AC procedures. This may involve processor dependent instalments of the smile correction, which accounts for the wavelength shifts in the MERIS cameras, the atmosphere and water models, conversion of water leaving radiance into fully normalised reflectance, or the vicarious adjustment. Potentially the latter could amplify the overall errors instead of reducing them, if the match-up data points are not homogeneously covered by pixels from all cameras. As match-up points have to be of exceedingly high quality, data points from cameras 1 and 2 covering the sun glint area are most likely excluded or under-represented.

The tests are designed to show any across-track angular dependencies which can lead to significant systematic errors in normalised water leaving reflectances and dependent products e.g. inherent optical properties (IOP) or chlorophyll concentration.

Due to the selection of data, the sun glint affected pixels are either removed by the individual quality flags of the processor or the combination of all algorithms' flags to attain the common best dataset. In all cases, the loss of data is not easily detected and the systematic error of the single processor does not influence the remaining data points in the comparison. The ForwardNN algorithm performs comparably well in the point-by-point analysis; as good as POLYMER and l2gen, depending on the choice of selected sites. Only investigations based on data, which covers the entire width of the swath, reveal and quantify the systematic erroneous behaviour, which would otherwise affect the creation of time series of merged products strongly.

References

Antoine, D., & Morel, A. (1998). Relative importance of multiple scattering by air molecules and aerosols in forming the atmospheric path radiance in the visible and near infrared parts of the spectrum. *Applied Optics, 37*, 2245–2259.
Antoine, D., & Morel, A. (1999). A multiple scattering algorithm for atmospheric correction of remotely sensed ocean color (MERIS instrument): Principle and implementation for atmospheres carrying various aerosols including absorbing ones. *International Journal of Remote Sensing, 20*, 1875–1916.
Antoine, D., & Morel, A. (2005). Atmospheric Correction of the MERIS observations Over Ocean Case 1 waters. *Technical Report. MERIS ATBD 2.7, Issue 5, Revision 0 December 2005.*
Antoine, D., & Morel, A. (2011). Atmospheric correction of the MERIS observations over ocean case 1 waters. *Technical Report. MERIS ATBD 2.7, Issue 5, Revision 5* (URL: http://envisat.esa.int/instruments/meris/atbd/atbd_2.7.pdf).
Doerffer, R., & Peters, M. (2006). MERIS regional case 2 water BEAM extension flags ATBD. *Technical Report.* GKSS Research Centre Geesthacht, Institute for Coastal Research.
Doerffer, R., & Schiller, H. (2007). The MERIS case 2 water algorithm. *International Journal of Remote Sensing, 28*, 517–535.
Feldman, G. C. (2008). URL: http://oceancolor.gsfc.nasa.gov/DOCS/MSL12/
Franz, B. A. (2012). Algorithm for retrieval of remote sensing reflectance from satellite ocean color sensors. URL: http://oceancolor.gsfc.nasa.gov/WIKI/AtmoCor.html
Franz, B. A., Bailey, S. W., Werdell, J., & McClain, C. R. (2007). Sensor-independent approach to the vicarious calibration of satellite ocean color radiometry. *Applied Optics, 46*, 5068–5082.
GCOS-154 (2011). Systematic observation requirements for satellite-based data products for climate. *Technical Report.* 7 bis, avenue de la Paix, CH-1211 Geneva 2, Switzerland: World Meteorological Organization (WMO).
Gordon, H., & Wang, M. (1994). Retrieval of water-leaving radiance and aerosol optical thickness over the oceans with SeaWiFS: A preliminary algorithm. *Applied Optics, 33*, 443–452.

D. Müller et al. / Remote Sensing of Environment 162 (2015) 257–270

Lerebourg, C., Mazeran, C., Huot, J., & Antoine, D. (2011). *Vicarious Adjustment of the MERIS Ocean Colour Radiometry. ATBD 2.24. ACRI.*

Moore, G., & Lavender, S. (2011). Case II. S bright pixel atmospheric correction. *Technical Report. MERIS ATBD 2.7, Issue 5, 2011* (URL: http://envisat.esa.int/instruments/meris/atbd/atbd_2.6.pdf).

Morel, A., & Gentili, B. (1996). Diffuse reflectance of oceanic waters. III. Implication of bidirectionality for the remote-sensing problem. *Applied Optics*, *35*, 4850–4862.

Morel, A., & Maritorena, S. (2001). Bio-optical properties of oceanic waters: A reappraisal. *Journal of Geophysical Research*, *106*, 7163–7180.

Müller, D. (2011). Geostatistical analysis of the chlorophyll distribution in the north sea based on Meris satellite data. URL: http://ediss.sub.uni-hamburg.de/volltexte/2011/5016/

Müller, D., & Krasemann, H. (2012). Product validation and algorithm selection report, part 1 — Atmospheric correction. *Technical Report AO-1/6207/09/I-LG D2.5. European Space Agency. ESRIN.*

Müller, D., Krasemann, H., Brewin, R. J., Brockmann, C., Deschamps, P. Y., & Doerffer, R. et . al (2015s). The Ocean Colour Climate Change Initiative: I. Methodology for an assessment of atmospheric correction processors based on in-situ measurements. *Remote Sensing of Environment*, *162*, 242–256.

Nelder, J. A., & Mead, R. (1965). A simplex method for function minimization. *Computer Journal*, *7*, 308–313.

Nobileau, D., & Antoine, D. (2005). Detection of blue-absorbing aerosols using near infra-red and visible (ocean colour) remote sensing observations. *Remote Sensing of Environment*, *95*, 368–387.

Steinmetz, F., Deschamps, P. Y., & Ramon, D. (2011). Atmospheric correction in presence of sun glint: Application to MERIS. *Optics Express*, *19*, 9783–9800.